Nano Energy 65 (2019) 103958

Contents lists available at ScienceDirect

Nano Energy

journal homepage: www.elsevier.com/locate/nanoen

Full paper

Photo-carrier extraction by triboelectricity for carrier transport layer-free photodetectors

Vincent K.S. Hsiao[a,b], Siu-Fung Leung[a], Yung-Chi Hsiao[c], Po-Kai Kung[a], Ying-Chih Lai[c], Zong-Hong Lin[d], Khaled N. Salama[a], Husam N. Alshareef[a], Zhong Lin Wang[e], Jr-Hau He[a,*]

[a] Computer, Electrical and Mathematical Sciences and Engineering, Physical Sciences and Engineering Division, King Abdullah University of Science and Technology, Thuwal, 23955-6900, Saudi Arabia
[b] Department of Applied Materials and Optoelectronic Engineering, National Chi Nan University, Nantou, 54561, Taiwan, ROC
[c] Department of Materials Science and Engineering, National Chung Hsing University, Taichung, 40227, Taiwan, ROC
[d] Institute of Biomedical Engineering, National Tsing Hua University, Hsinchu, 30013, Taiwan, ROC
[e] School of Materials Science and Engineering, Georgia Institute of Technology, Atlanta, GA, 30332-0245, USA

ARTICLE INFO

Keywords:
Triboelectricity
Photo-carrier extraction
Charge transport layer
Photodetector

ABSTRACT

Efficient carrier extraction is essential for high performance optoelectronic devices, such as solar cells and photodetectors. Conventional strategies to separate photogenerated carriers typically involve the fabrication of a p-n junction by doping and the use of carrier selective charge transport layers. However, these techniques often require high temperature processes or costly materials. In this work, we demonstrate an innovative and simple approach of extracting photogenerated carriers from organometallic halide perovskites utilizing triboelectricity. The triboelectric device can be easily fabricated at low temperature using inexpensive materials on plastic substrates, enabling it to be readily integrated into self-powered optoelectronic devices. As a proof-of-concept, we fabricated a triboelectrics-assisted perovskite photodetector, which enabled us to study the surface charges generated using different electrical contacts and bending conditions performed by the device. With the assistance of a triboelectric charge-induced electric field, the photocurrent and transient photoresponses were significantly enhanced. Furthermore, we integrated the plastic triboelectric device with a flexible photodetector to demonstrate this carrier collection approach in flexible/wearable electronics. To the best of our knowledge, this work is the first report of carrier extraction in organometallic halide perovskite photodetector by triboelectric charges, demonstrating a potential use for carrier extraction in other semiconductor-based optoeletronic devices.

1. Introduction

The performances of electronic/optoelectronic devices are determined by the mobile carriers (electrons in the conduction band and holes in the valence band). There are different ways to generate mobile carriers, including thermal generation, photo generation, impact ionization, and field emission according to the energy supplied in the process [1]. The different mechanism of carrier generation leads to a variety of device applications, including thermoelectric devices, solar cells, photodetectors, Zener diodes, avalanche photodiodes, and tunnel diodes [1]. However, to avoid electrical losses due to carrier recombination and achieving high performance of electronic/optoelectronic devices, efficient carrier extraction or separation is of particular importance. Typical way is done by intentionally formed p-n junction since the recombination that occurs in the depletion region of the junction is less significant due to the high carrier drift velocity [1]. With the assistance of the built-in electric field established by the p-n junction, the electron and holes are driven toward to the contact electrodes. Note that the doping for junction formation usually involves high temperature processes, which are costly and time consuming [2].

Additionally, several strategies are used to further improve the carrier extraction from the devices, depending on the material system, device configuration, and the specific application. For example, heterojunction solar cells, including dye-sensitized and organometallic halide perovskite-based photovoltaics [3–10], has advantages with low temperature and solution-based fabrication processes, but the layering steps are time consuming, and extra attention is needed to be paid on the junction interfaces. The main purpose for layering process is for incorporating the electron/hole transport layers to efficiently enhance the charge separation and further increase the photocurrent [11–17].

* Corresponding author.
E-mail address: jrhau.he@kaust.edu.sa (J.-H. He).

https://doi.org/10.1016/j.nanoen.2019.103958
Received 15 June 2019; Received in revised form 22 July 2019; Accepted 30 July 2019
Available online 02 August 2019
2211-2855/

For the organometallic halide perovskite photodetectors (PDs) [6,6],-phenyl-C61-butyric acid methyl ester (PCBM) and spiro-OMeTAD are often used as electron and hole transport layers, respectively [18–24]. However, these organic based charge transport layers are unstable under light irradiation [25]. The interfaces between the light-absorbing material and the electron/hole transport layers must be handled carefully to prevent defects or cracking. In addition, the material costs for these charge transport layers are relatively high and require expensive and slow deposition processes. Therefore, photo-carrier extraction by such an approach poses a challenge for the fabrication of high-performance, stable and cost-effective optoelectronic devices. It has been widely reported that a well-defined junction interface is required to avoid recombination during carrier transfer [26]. A well-structured interface of hybrid materials largely enhances charge separation and transfer efficiency [27]. The efficiency of electron/hole pair separation and collection is determined by whether the carriers can diffuse into the depletion regions. Radial junction architectures feature short collection distance, and ideally they can have charge collection efficiencies near unity and thus are highly defect tolerant [28–32].

Recently, tribotronics has been proposed and demonstrated as a new field of hybrid optoelectronic device which couples the triboelectricity and semiconductor devices [33]. The application of tribotronics allows semiconductor devices actuated by mechanical motion and interacted between human or ambient. The triboelectronic nanogenerator (TENG) can convert mechanical energy generated by human motion, or energy from the ambient including wind or water wave energy into electricity. The triboelectric charges are generated due to the charge transfer between two materials that exhibit distinct surface electron affinity, and the open-circuit potential results from the separation of the triboelectric charges [34–37]. In this work, we explore a novel approach to extract photo-carriers inside a solution-processed organometallic halide perovskite thin film using the triboelectricity of simple device design. Previous demonstrations of halide perovskite photovoltaics need electron/hole transport layers to resolve the instability issues of halide perovskite as photoactive material [25]. No matter which kinds of ways to solve the unstable issue of halide perovskite, the electron/hole transport layers still are required in the layered structure. Here, the simple triboelectric device is consisted of two indium tin oxide (ITO)-coated polyethylene terephthalate (ITO-PET) substrates to generate triboelectricity which extract photo-generated carriers. Comparing to typical use of additional fabrication of electron/hole transport layers in perovskite PD, the use of TENG is robust and cost-effective. The TENG-actuated perovskite PD on a flexible substrate is fabricated by solution-processed methods that the halide perovskite thin film was sandwiched between the gold (Au) and ITO electrodes (Au/perovskite/ITO). The triboelectrification of TENG generates positive and negative charges which accumulate on the perovskite PD's electrodes. The electrostatic charges attract and separate the electron/hole pairs upon light illumination. We rigorously investigate the working principle by characterizing the optoelectronic performance from TENG-actuated perovskite PD. Under light illumination, the photo-generated electron/hole pairs could be separated by the potential difference, which previously created by TENG, on the top and bottom electrode/perovskite interface. The controlled experiments of using DC voltage as potential difference to separate photo-carriers have been conducted showing only TENG-generated triboelectricity can help the charge carrier separation. Moreover, we studied the optoelectronic characteristics of the perovskite PD under different triboelectric potential and bending conditions of the TENG. Notably, the photocurrent and response time of the PD is found to be enhanced by triboelectricity. Since the TENGs are composed with flexible polymer substrates, we construct a triboelectric-actuated PD consisted of a TENG and a flexible Au/perovskite/ITO PD. Further demonstration shows that under low light condition, the mechanical bending can only actuate TENG-assisted perovskite PD. Those experimental results suggest the triboelectricity can be a novel and cost-effective approach for extracting photo-carriers and eliminating the need of unstable carrier transport layers. Meanwhile, such approach may bring possible application to fabricate flexible semiconductor solar cell without the use of p-n junction to extract photo-generated carriers.

2. Results and discussion

2.1. Characteristics of perovskite thin film

The light-absorbing materials used in the PD device is the solution-processed $(C_4H_9NH_3)_2PbBr_4$ perovskite thin film, (fabrication details are described in the Methods section), sandwiched between an ITO-PET substrate (15 mm × 15 mm in size) and a gold electrode deposited by e-beam evaporation. Fig. S1a shows the top-view scanning electron microscopy (SEM) image of the perovskite film. The cross-sectional SEM image of the perovskite layer (Fig. S1b) suggests a multi-layered, two dimensional network inside the 1 μm thick perovskite thin film possibly due to the 2D perovskite structure of the $C_4H_9NH_3Br$ precursor [38,39]. Fig. S1c shows the photoluminescence (PL) and absorption spectrum of the perovskite film indicating a sharp absorption edge at 530 nm (2.3 eV) and a PL peak located at 548 nm.

2.2. Working principle of TENG-assisted perovskite PD

The schematics of PD coupled with TENG and the working principle of the photo-carrier extraction by triboelectricity are shown in Fig. 1. The TENG is composed of two ITO-PET substrates and connected to the sandwiched Au/perovskite/ITO electrodes. The working principle of TENG is as follow. When the ITO is in contact with PET which tends to

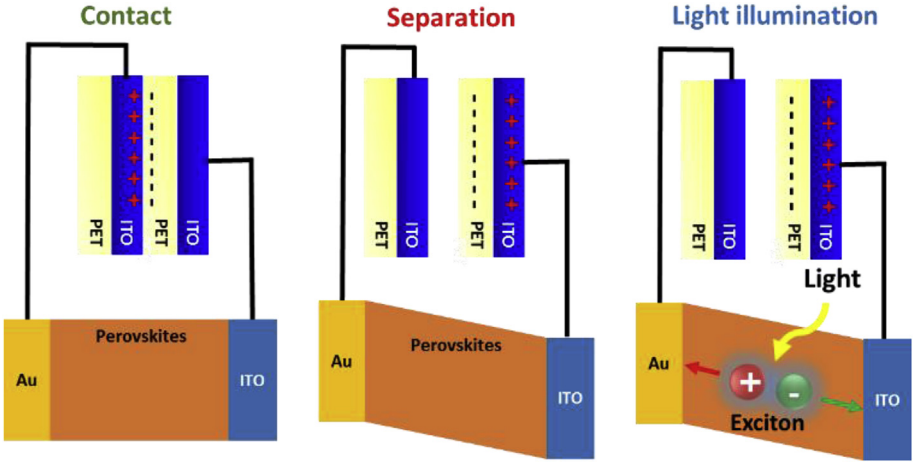

Fig. 1. Triboelectric-assisted carrier extraction and separation in perovskite PD. The schematic of a triboelectric-assisted perovskite PD showing charge carrier separation assisted by the triboelectric charges created by the TENG. The surface charge generated from the application of TENG is finished before the light illumination.

attract electrons, electrons flow from ITO to the PET, resulting in the positively charged ITO. When the two ITO-PET substrates separate, the open circuit (V_{oc}) potential is established due to the charge neutralization on the ITO surfaces [40–42]. We characterize the V_{oc} of the TENG which is mechanically triggered by a linear motor [37] as shown in Fig. S2. The positive and negative triboelectric charges accumulate at the interfance between perovskite semiconducting material and Au or ITO electrodes [43] of the perovskite PD, as a result, a potential difference is established across the perovskite layer. When the perovskite PD is illuminated by light and generating photo-carriers, the TENG-generated potential difference separates the photo-carriers (electron-hole pairs) and prevents the carrier recombination inside the perovskite layer. During the experiments, the positive charged terminal of the TENG can be connected to either ITO or Au electrode of the perovskite PD. Figs. S3a and S3b show the detailed circuit diagram of the electrical connection and schematic of the Au/perovskite/ITO PD device for measuring the current-voltage (*I–V*) characteristics under dark and light conditions. Here, the "(+) triboelectrics" symbol represents the positive charge (+) being connected to the ITO electrode of the PD, while the "(−) triboelectrics" symbol represents that the negative charge (−) is connected to the Au electrode. All *I–V* curves are obtained under the forward bias condition after mechanical movement by finger tapping applying on the TENG (see Supporting Movie I).

Supplementary video related to this article can be found at https://doi.org/10.1016/j.nanoen.2019.103958.

2.3. *I–V* performance of TENG-assisted perovskite PD

To explore the working principle of triboelectric-assisted perovskite PD, the charge carrier dynamic at the junction interfaces of the PD with the help of triboelectricity is discussed. Fig. 2a compares the dark current of the perovskite PD with and without applying triboelectric charge under different circuit connections. Without the use of electron/hole transport layers, the *I–V* behavior of the perovskite PD, as shown in Fig. 2a (white curve), can be considered as a Schottky junction formed at the interfaces between the electrodes and the semiconducting perovskite [44]. The schematic of band diagram is shown in Fig. 2b. The values of energy level of conduction and valence band are from the previous report [45]. When a forward bias (V_{for}) is applied, it lowers Schottky barrier height and thus facilitates the charge carrier collection by the Au and ITO electrodes, resulting in increased current. The *I–V* curve measured from the triboelectric-assisted perovskite PD with (+) triboelectric connection shows an improved performance as compared to the control sample when the applied forward bias is higher than 0.3 V. In contrast, applying the (−) triboelectric connection decreases the current by 2 orders of magnitude, hence decreasing the performance of the device. The enhanced current from the triboelectric-assisted PD can be explained by the energy band alignment of the Au/perovskite/ITO device. Since the work function of Au is higher than that of ITO, electrons are facilitated to flow into the ITO electrode under V_{for} [46]. The application of the (+) triboelectric charge results in holes and electrons accumulating at the ITO and gold electrodes, respectively, as shown in Fig. 2c. The accumulated charges, which serve the same role as the electron/hole transport layers in a typical perovskite PD, help separating the photo-generated electron/hole pairs and contribute to the photocurrent. In contrast, the application of (−) triboelectric condition results in electrons accumulating the ITO electrode and holes on the Au electrode, as shown in Fig. 2d. The accumulated charges, which could be considered as the reverse biased condition, increase the Schottky barrier height and thus preventing photo-generated electron/hole pairs separation; therefore a lower photocurrent is observed under the (−) triboelectric connection. Note that before the illumination, the dark current (I_{dark}) from the (+) triboelectric-assisted perovskite device at zero bias is almost 10 times larger than that measured from the control, as shown in Fig. 2a. The I_{dark} from the (+) triboelectric-assisted perovskite device is also slightly higher than the control when applying the forward bias. Fig. 3a shows the *I–V* curve of the control perovskite PD measured with and without illumination. Without illumination, a built-in potential is generated at the electrode-semiconductor interfaces. Under illumination, the photo-generated electrons and holes are collected by the Au and ITO electrodes, resulting in the observation of a photocurrent (I_{light}). Fig. 3b shows the *I–V* curves measured from the (+) triboelectric-assisted perovskite PD under dark and illuminated conditions. Interestingly, the I_{light} at zero bias was almost 100-times

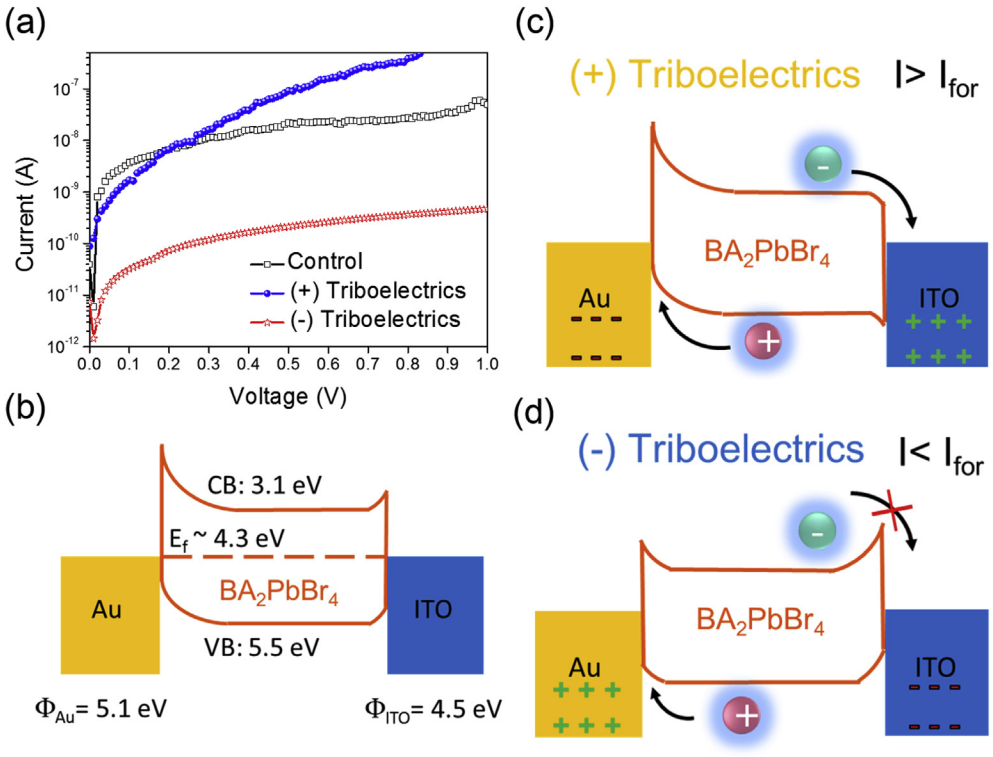

Fig. 2. The performance and band diagram of perovskite PD under different format of triboelectricity and electric connection. (a) Forward biased *I–V* characteristics of the Au/perovskite/ITO PD under (+) and (−) triboelectric charge conditions. Schematic of the energy levels of the Au/perovskite/ITO PD featuring the formation of a Schottky barrier between the perovskite and Au/ITO electrodes for the electric connection of (b) no TENG connected, (c) (+) triboelectric connection, and (d) (−) triboelectric connection.

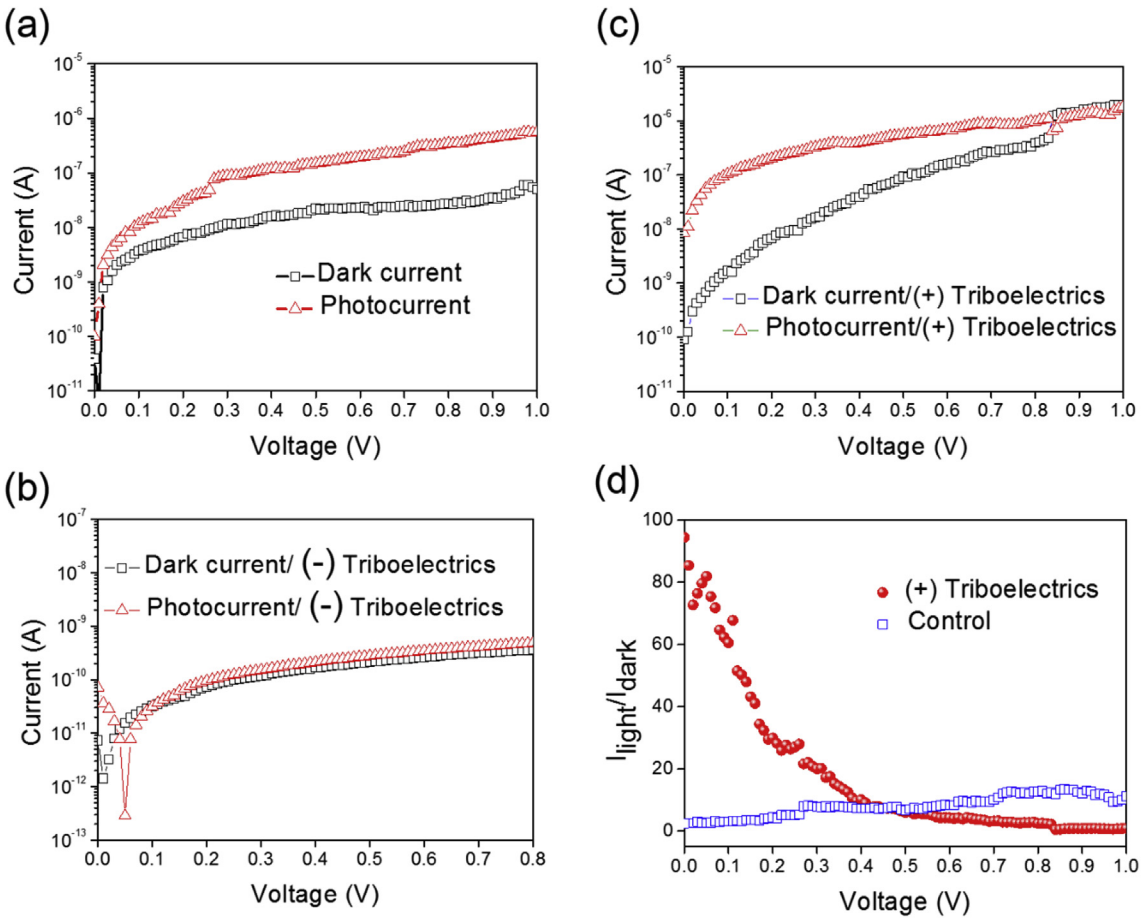

Fig. 3. Current-voltage analysis of perovskite PD under different format of triboelectricity corresponded to different electric connection between PD and source meter. (a) *I–V* curve for Au/perovskite/ITO PD control device (without triboelectricity) and (b) the (+) triboelectric-connected Au/perovskite/ITO PD measured at an applied forward bias from 0 to 1 V in the dark and under 10 mW/cm^2 white light illumination. (c) Forward biased *I–V* curve of the (−) triboelectric-assisted Au/perovskite/ITO PD in the dark and under 10 mW/cm^2 white light illumination. (d) Forward-biased dependent photocurrent enhancement of the (+) triboelectric-assisted PD.

larger than I_{dark}. The generated charges from the application of the (+) triboelectric condition create an electrostatic potential that promotes the photocurrent without the external V_{for}. However, under illumination, the I_{light} measured from the (−) triboelectric-assisted device was the same as I_{dark}, as shown in Fig. 3c, regardless of external V_{for}. This suggests the application of the (−) triboelectric turns off the perovskite PD because the triboelectrics-generated surface electrostatic charges of opposite sign prevents the photo-generated carriers flowing into the electrodes.

To evaluate the effect of triboelectricity on the perovskite PD under an external forward bias, we calculate the value of I_{light}/I_{dark} for the triboelectric-assisted perovskite PD and control device, as shown in Fig. 3d. The (+) triboelectric-assisted device generates the largest value of I_{light}/I_{dark}, due to the (+) triboelectric condition providing additional electrical potential to lower the Schottky barrier height and facilitate charge separation. However, the I_{light}/I_{dark} value decreases with increasing applied voltage, which is in contrast with the control sample, as shown in Fig. 3a. For the control, the ability to separate charges increases with increasing external voltage, in which case I_{light}/I_{dark} increases with applied voltage. For the case of the (+) triboelectric-assisted perovskite PD, an external forward bias reduces the triboelectric effect, so that when V_{for} is larger than 0.5 V, the value of I_{light}/I_{dark} of the control sample was actually larger than the (+) triboelectric-assisted device. These results demonstrate that the application of triboelectricity is surely beneficial in self-biased optoelectronic device.

2.4. Band alignment and photocurrent changes due to the effect of triboelectricity

Fig. 4a shows the schematic of band alignment of the (+) triboelectric-assisted perovskite PD. Before illumination, the perovskite PD is treated with triboelectric charge and the two electrodes (Au and ITO) are full of positive/negative charges provided by TENG. Under illumination, the lower Schottky barrier makes the photo-generated holes migrate to the Au/perovskite interface, leaving behind the unpaired electrons in the perovskite/ITO interface and contributing to the photocurrent. The generation of surface charges on the Au and ITO electrodes due to the application of TENG results in enhanced photocurrent and photoresponse.

To quantify the triboelectric effect on the perovskite PD device, the *I–V* curves are measured under different open circuit voltage (V_{oc}) supplied by the TENG. The V_{oc} was generated by continuously contact-separation movement controlled by a linear motor. The result (Fig. 4b) shows that the V_{oc} under 60 V has no obvious effect on the PD performance and higher V_{oc} (100 V) decrease the performance of the perovskite PD. The reason can be attributed to that large amount of positive and negative charges filled defects inside the perovskite film which facilitate the photon-generated charge recombination and decrease the photocurrents. To verify the surface changes supplied by the TENG prevents the photo-generated charge recombination, we measure the photocurrent under the connected and disconnected circuit condition between TENG and perovskite PD illuminated with 10 mW/cm^2 white

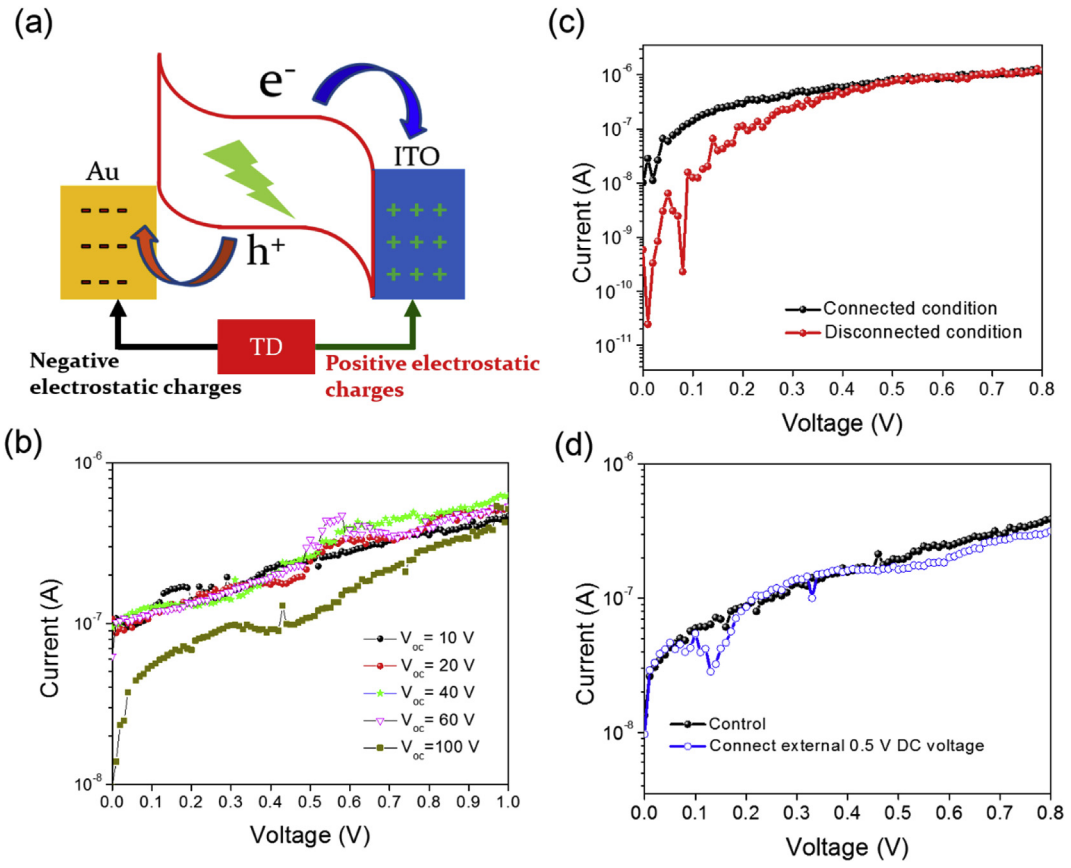

Fig. 4. Working mechanism of perovskite PD and the *I–V* characteristics of PD under different triboelectricity and DC voltage. (a) Schematic diagram and the working principle of the (+) triboelectric-assisted perovskite PD. The device is pre-trated with TENG; therefore, the surface charges are accumulated on Au and ITO electrode, separately. Under light illumination, the energy band alignment of the Au/$(C_4H_9NH_3)_2PbBr_4$/ITO and positive/negative carriers transfer to Au and ITO separately. *I–V* characteristic of Au/perovskite/ITO PD under (b) different open circuit voltage supplied by the TENG, (c) without and with electric connection of TENG, and (d) without (control) and with supplying external DC voltage of 0.5 V.

light. Decreased photocurrent is observed by disconnecting the circuit between TENG and perovskite PD when the V_{for} is less than 0.5V, as shown in Fig. 4c. The TENG did provide the electrostatic charges to prevent the photo-generated charge recombination inside perovskite and increase the photocurrents. We also observe that when the applied external V_{for} is higher than 0.5 V, the photocurrents observed in both circuit connections are the same and the result is similar as shown in Fig. 3d. It should be attributed to the use of triboelectricity which provides the electrical potential and the case is different from the use of external V_{for}. To further examine the difference, we use a DC voltage power supply being connected in parallel with the perovskite PD to replace the role of TENG and measure the dark current and photocurrent (Fig. 4d). The result shows no enhancement of photocurrent observed from perovskite PD treated with external DC voltage.

2.5. *Transient and spectral photoresponse of TENG-assisted perovskite PD*

We now understand that the triboelectricity can prevent the recombination of photo-generated carriers and enhance the photocurrents. Also, the performance of perovskite PD can be enhanced by TENG under zero external voltage. We can directly measure the photocurrent from perovskite PD which is treated with triboelectricity previously under light illumination without external bias. Fig. 5a shows the transient photoresponse (photocurrent) of the Au/perovskite/ITO PD without charge transport layers. The photocurrent is measured by periodically blocking the white light source. The resulting photocurrent increases slowly without saturating and rapidly drops to zero when the light is OFF. When the light is turned on again, the unsaturated photocurrent is again observed but becomes higher than the value obtained from the previous cycle. The increased photocurrent is due to that the photo-generated holes are recombined inside the perovskite film. An excess of electron concentration leads to the higher photocurrent due to the lack of electron/hole transport layers. The defects inside perovskite film could also be the reason of slow charge recombination [25,45] resulting non-saturated photocurrent. Fig. 5b shows the photoresponse of the TENG-assisted perovskite PD under the same condition of white light illumination. The photocurrent saturates more rapidly and is higher as compared to the control due to the generation of positive and negative triboelectric charges to separate photocarriers. The triboelectric charges prevent the photo-carriers being trapped and recombined inside the perovskite film, thus facilitating the carrier drift to the electrodes.

Previous studies have indicated that the exciton band of spectral response from perovskite PD blue-shifts with external voltage [47, 48]. To verify the effect of triboelectricity on perovskite PD, we characterized the spectral response of the triboelectric-assisted Au/perovskite/ITO PD and the controlled sample, as shown in Fig. 5c. The photocurrent spectral response (i.e., photoresponsivity) of the controlled PD (without applying TENG) at zero external bias shows a strong and narrow exciton band at 535 nm with a full width at half maximum of 20 nm and a broad photoresponse region correlated to the band-to-band transitions [49]. The strong and narrow spectral response matches the absorption band edge of the perovskite reported previously. Compared to the control PD, the photocurrent response measured from the TENG-assisted PD increases in the entire spectral range (400–900 nm); however, the peak wavelength and bandwidth of the exciton band remained

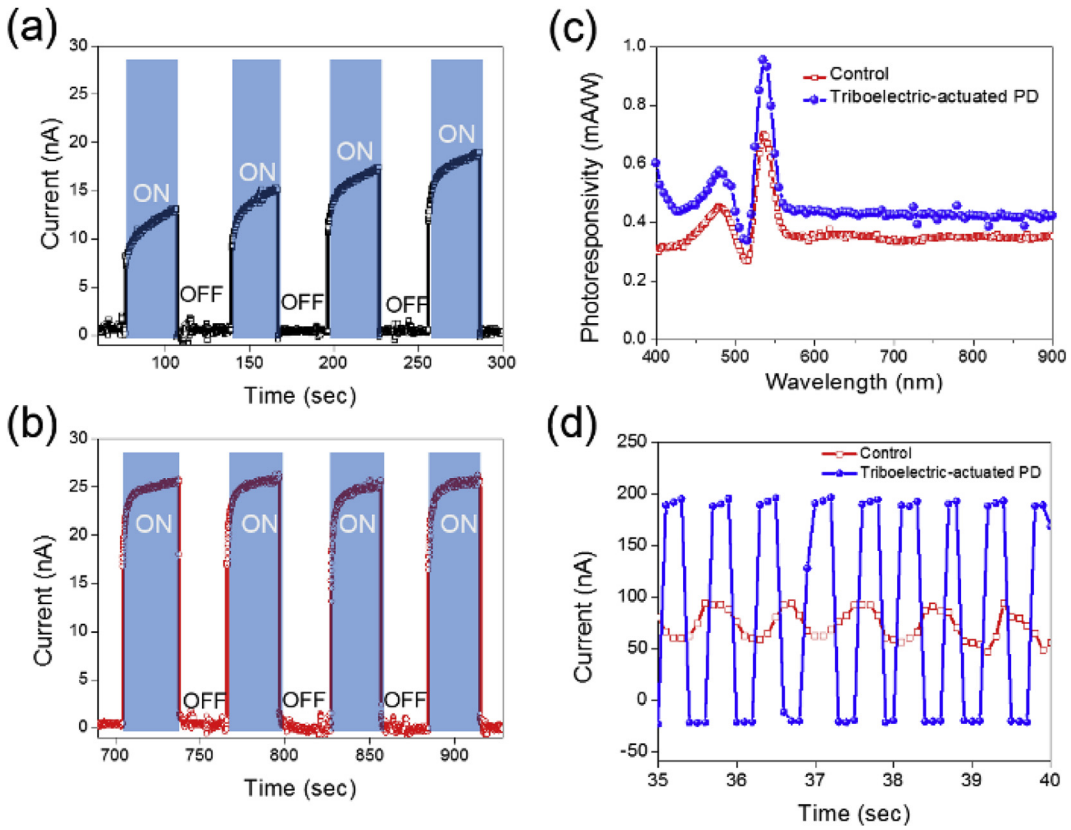

Fig. 5. The transient and spectral photoresponse and of the Au/perovskite/ITO PD under ON-OFF light illumination. The white light of 10 mW/cm^2 was illuminated on the perovskite PD (a) without applying triboelectric friction and (b) with applying triboelectricity. (c) Enhanced spectral photoresponsivity measured from triboelectric-actuated perovskite PD under 50 mW laser of 532 nm wavelenth. (d) The transient photoresponse of the triboelectric-actuated perovskite PD (blue) and perovskite PD without assistance of triboelectricity (red) under alternating ON-OFF laser light (50 mW) illumination with a 3 Hz chopping frequency. The V_{oc} for TENG is measured as 50 V. All measurements were carried out without applying external voltage.

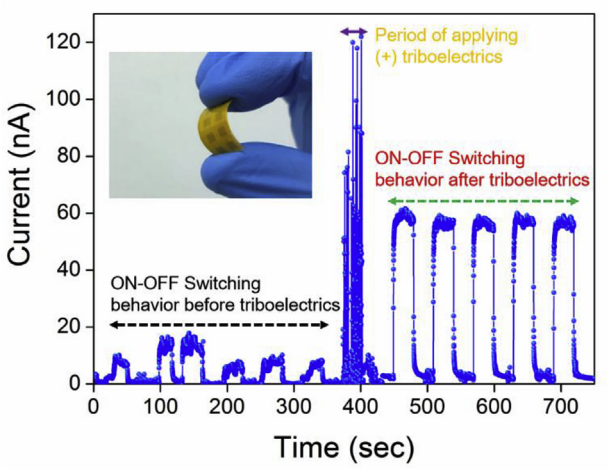

Fig. 6. Transient photocurrent observed from TENG-assisted perovskite in bending condition. Photoresponse of the bent Au/perovskite/ITO PD under ON-OFF switching of 20 mW/cm^2 white light illumination. The inset is an image of the flexible Au/perovskite/ITO PD.

unchanged. Moreover, the photocurrent response observed from the TENG-assisted PD shows no substantial variation in term of spectral position and width. These behaviors indicate that the assistance of triboelectricity correlated with the increased photocurrent spectral response.

Without charge transport layers or applying external voltage, the photocurrent of a perovskite PD is normally unstable due to charge recombination inside the active material. We can evaluate the stability of the PD by continuously switching the illumination on and off and measuring the photocurrent at the same time. Fig. 5d shows the transient photocurrent response of the PD with (blue)/without (red) triboelectricity under the chopping frequency of 3 Hz using a 532 nm and 50 mW laser as illumination. A schematic of the optical setup is shown in Fig. S4a. Apparently, the photocurrent measured from the triboelectric-assisted PD changes rapidly with the chopping frequency, as shown and the controlled sample cannot. When the light turns ON, the photocurrent observed from TENG-assisted perovskite PD suddenly increases to 200 nA which is almost 50 times larger than the value observed from control sample. The transient photocurrent at different optical chopping frequencies for the PD assisted with triboelectric charges are shown in Figs. S4b and S4c. The results demonstrate that triboelectricity can effectively improve the photoresponse of the perovskite PD in on-off switching of light illumination.

2.6. Self-powered performance of TENG-assisted PD at bending condition

One of the advantages of utilizing triboelectricity for carrier extraction is the compatibility of the polymer substrate-based TENG in the applications of flexible and wearable electronic devices. Previous reports have shown the fairly stable flexible perovskite PDs based on a layered design which utilizing organic electron/hole transport layers [37,43]. However, the fabrication of these layers involves costly processes, making it difficult to produce a flexible perovskite PD that is stable under bending conditions. Fig. 6 (inset) shows an image of the flexible Au/perovskite/ITO PD with a bending radius of 2 cm. Without the assistance of an external voltage or TENG, the photoresponse of the device is not stable under alternating light illumination (Fig. 6).

However, a reproducible and stable photocurrent is observed from the perovskite PD when it is assisted by the TENG before photocurrent measurement. The TENG effectively replaces the role of an external voltage and electron/hole transport layers when using the perovskite PD at bent condition.

Finally, we incorporated the TENG with the perovskite PD into a single, flexible device and actuate TENG component by bending the entire structure. Bending the simple design of TENG which is consisted of only two ITO-PET substrates, cannot provide enough triboelectric charges; therefore, we inserted a polytetrafluoroethylene (PTFE) layer between the ITO and PET to enhance the triboelectricity [47]. The enhancement is due to the difference of tendency of the two materials to charge positively (lose electron) or negatively (gain electron). PTFE has a higher tendency to gain electron than PET, thus enhancing the generated triboelectric charge [32]. We then integrated this ITO-PTFE/PET TENG into the plastic Au/perovskite/ITO PD (Fig. S5a) by simply binding all substrates as a piece of bendable triboelectric-actuated perovskite PD. The output V_{oc} from ITO-PTFT/PET TENG is shown in Fig. S5b and in Supporting Movie II. The V_{oc} can be continuously turned on and off by repeatedly bending the device. The bending induces friction between ITO and PTFE and further creates the positive and negative electrostatic charges flowing into the Au/ITO electrodes. The surface electrostatic charges help prevent the photo-carriers from recombining in the perovskite thin film and enhance the photocurrent. Fig. 7 shows the images of the flexible PD at different states of supplying triboelectric charges and light illumination. Photocurrent can only be observed when triboelectric charges is supplied by bending the TENG. We record the whole process of bendable triboelectric-assisted perovskite PD in Supporting Movie III.

Supplementary video related to this article can be found at https://doi.org/10.1016/j.nanoen.2019.103958.

3. Conclusions

We have proposed a simple and novel approach for extracting photo-generated carriers in optoelectronic devices using triboelectricity, and have successfully demonstrated the concept on a triboelectric-assisted perovskite PD. Without the need of fabricating organic/inorganic electron/hole transport layers, the triboelectric-assisted perovskite PD can generate a high and stable photoresponse comparing with same PD without triboelectricity. We explain the principle of photo-carrier extraction and verify it by characterizing the PD using (+) and (−) triboelectric connection. The TENG produces the triboelectric charges through friction generated by mechanical motion of contact/separation or bending between two ITO/PET or ITO/PTFE substrates. The triboelectric charges help to achieve the stable and reproducible photocurrent by improving the charge carrier separation as compared to the control sample without the use of carrier transport layers. Moreover, by integrating a TENG with a perovskite PD into a whole flexible device, we can actuate the photoresponse by mechanical bending. Photo-carrier extraction by triboelectricity has the advantages of simple and low-cost fabrication. The durable and self-powered nature of such hybrid design suggests the further development in flexible and wearable optoelectronic devices.

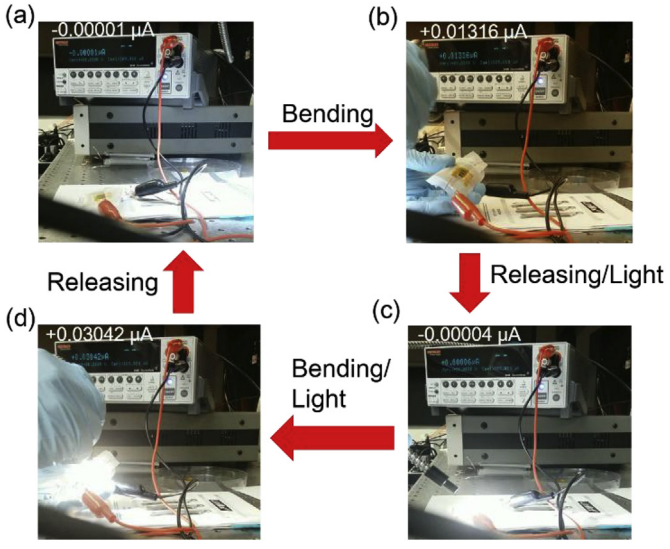

Fig. 7. Working sequence of the mechanical bending-actuated perovskite PD. (a) At the initial status, without bending or illumination, no dark current is detected. (b) A bending force results in surface triboelectric charges, as recorded by the current meter. (c) Releasing the bending force and illuminating the PD results in no photocurrent being measured. (d) The generation of triboelectric charges due to the bending force facilitates the separation of photo-generated carriers, resulting in a photocurrent.

4. Methods

4.1. Material and device fabrication

The (C4H9NH3)2PbBr4 thin films were prepared using a modified co-solvent assisted method, as reported previously [27]. All the solution preparation and solution-processed thin film growth was carried out inside a fume hood. C4H9NH3Br (154 mg) was synthesized following a previous report [27] and PbBr2 (190 mg, 99.999%) was purchased from Sigma-Aldrich. These reagents were first dissolved in 4 mL co-solvent, containing 2 mL dimethylformamide (anhydrous, 99.8%) and 2 mL chlorobenzene (anhydrous, 99.8%), all purchased from Sigma-Aldrich and used without further purification. 40 μL of this mixed solution was then added onto a commercially available ITO-coated PET substrate featuring 25 Ω/sq surface resistivity. A spin coating method was applied to create the perovskite thin film while the substrate was heated at 70 °C on a hot plate for 1 h. We deposited Au electrodes of 40 nm thickness by sputtering as the top electrode on the perovskite. The TENG powered by finger tapping was fabricated using two 10 mm × 10 mm ITO-coated PET substrates. The TENG powered by bending for the all-flexible PD was fabricated using a PTFE substrate inserted between the two ITO coated PET layers of the combined device (Fig. S12a). The Au/perovskite/ITO PD was connected to both types of triboelectric devices by copper wires, which were connected to the electrodes using 3 M tape.

4.2. Morphology, electrical, and optical characterization

A field emission SEM was used to acquire the surface and cross-sectional images of the perovskite thin film. The UV–Vis absorption spectrum of (C4H9NH3)2PbBr4 was recorded with a Varian Cary 6000i spectrophotometer. The I–V curve measurements were performed on a probe station connected to a Keithley 4200 or Keithley 2400 source meter. The spectral photoresponsivity measurements were performed at room temperature employing a light source (100 W halogen lamp) equipped with a monochromator (Acton SP2155) and a current meter (Keithley 6485). The spectral photoresponsivity of the Au/perovskite/ITO PD was determined relative to the value measured from a standard silicon PD (DET10A, Thorlabs). The transient photoresponses were measured with a current meter (Keithley 6485) using a 100 mW, 532 nm laser light at different chopping frequencies.

Author contributions

V·K·S·H and S.L conceived the idea and wrote the paper. V.K.S.H designed the TENG-assisted perovskite photodetector, performed the materials and devices characterization and analysis. Y.H., Y. L, Z.L. performed the triboelectric performance tests and analyzed the mechanisms. P.K. helped the farbication of device and photodetecting

measurement. K.N.S, H·N.A, and Z.L.W provided experimental directions. J.H. supervised this project. All authors discussed the results and commented on the manuscript.

Competing financial interests

The authors declare no competing interests.

Acknowledgements

This work was financially supported by the King Abdullah University of Science and Technology (KAUST) Office of Sponsored Research (OSR) (OSR-2016-CRG5-3005), KAUST solar center (FCC/1/3079-08-01), KAUST Sensor Initiative, KAUST baseline funding, and the Ministry of Science and Technology (MOST), Taiwan, under project number MOST-107-2221-E-260-016-MY3.gs5

Appendix A. Supplementary data

Supplementary data to this article can be found online at https://doi.org/10.1016/j.nanoen.2019.103958.

References

[1] D.A. Neamen, Semiconductor Physics and Devices : Basic Principles, McGraw Hill, 1992.
[2] G.S. May, C.J. Spanos, Fundamentals of Semiconductor Manufacturing and Process Control, IEEE; Wiley-Interscience, 2006.
[3] W. Tian, H.P. Zhou, L. Li, Small 13 (2017) 1702107.
[4] X.M. Li, D.J. Yu, J. Chen, Y. Wang, F. Cao, Y. Wei, Y. Wu, L. Wang, Y. Zhu, Z.G. Sun, J.P. Ji, Y.L. Shen, H.D. Sun, H.B. Zeng, ACS Nano 11 (2017) 2015–2023.
[5] W.H. Wang, Y.R. Ma, L.M. Qi, Adv. Funct. Mater. 27 (2017) 1603653.
[6] L. Shen, Y.J. Fang, D. Wang, Y. Bai, Y.H. Deng, M.M. Wang, Y.F. Lu, J.S. Huang, Adv. Mater. 28 (2016) 10794–10800.
[7] Y. Lee, J. Kwon, E. Hwang, C.H. Ra, W.J. Yoo, J.H. Ahn, J.H. Park, J.H. Cho, Adv. Mater. 27 (2015) 41–46.
[8] H.J. Snaith, J. Phys. Chem. Lett. 4 (2013) 3623–3630.
[9] J.Y. Jeng, Y.F. Chiang, M.H. Lee, S.R. Peng, T.F. Guo, P. Chen, T.C. Wen, Adv. Mater. 25 (2013) 3727–3732.
[10] G. Hodes, Science 342 (2013) 317–318.
[11] M.A. Loi, J.C. Hummelen, Nat. Mater. 12 (2013) 1087–1089.
[12] M.M. Lee, J. Teuscher, T. Miyasaka, T.N. Murakami, H.J. Snaith, Science 338 (2012) 643–647.
[13] K.T. Ho, S.F. Leung, T.Y. Li, P. Maity, B. Cheng, H.C. Fu, O.F. Mohammed, J.H. He, Adv. Mater. 30 (2018) 1804372.
[14] D.J. Joe, S. Kim, J.H. Park, D.Y. Park, H.E. Lee, T.H. Im, I. Choi, R.S. Ruoff, K.J. Lee, Adv. Mater. 29 (2017) 1606586.
[15] L. Dou, Y.M. Yang, J. You, Z. Hong, W.-H. Chang, G. Li, Y. Yang, Nat. Commun. 5 (2014) 5404.
[16] N.J. Jeon, J.H. Noh, Y.C. Kim, W.S. Yang, S. Ryu, S.I. Seok, Nat. Mater. 13 (2014) 897–903.
[17] Y. Huang, E.J. Kramer, A.J. Heeger, G.C. Bazan, Chem. Rev. 114 (2014) 7006–7043.
[18] K.A. Mazzio, C.K. Luscombe, Chem. Soc. Rev. 44 (2015) 78–90.
[19] C.X. Bao, W.D. Zhu, J. Yang, F.M. Li, S. Gu, Y.R.Q. Wang, T. Yu, J. Zhu, Y. Zhou, Z.G. Zou, ACS Appl. Mater. Interfaces 8 (2016) 23868–23875.
[20] Y.W. Li, L. Meng, Y. Yang, G.Y. Xu, Z.R. Hong, Q. Chen, J.B. You, G. Li, Y. Yang, Y.F. Li, Nat. Commun. 7 (2016) 10214.
[21] O. Malinkiewicz, A. Yella, Y.H. Lee, G.M. Espallargas, M. Graetzel, M.K. Nazeeruddin, H.J. Bolink, Nat. Photonics 8 (2014) 128–132.
[22] G.E. Eperon, V.M. Burlakov, P. Docampo, A. Goriely, H.J. Snaith, Adv. Funct. Mater. 24 (2014) 151–157.
[23] P. Docampo, J.M. Ball, M. Darwich, G.E. Eperon, H.J. Snaith, Nat. Commun. 4 (2013) 2761.
[24] Q.S. An, F.J. Zhang, J. Zhang, W.H. Tang, Z.B. Deng, B. Hu, Energy Environ. Sci. 9 (2016) 281–322.
[25] S. Rafique, S.M. Abdullah, W.E. Mahmoud, A.A. Al-Ghamdi, K. Sulaiman, RSC Adv. 6 (2016) 50043–50052.
[26] H.P. Wang, J.-H. He, Adv. Energy Mater. 7 (2017) 1602385.
[27] S.F. Leung, Q. Zhang, M.M. Tavakoli, J.-H. He, X. Mo, Z. Fan, Small 12 (2016) 2536–2548.
[28] A.I. Hochbaum, P.D. Yang, Chem. Rev. 110 (2010) 527–546.
[29] S.H. Tsai, H.C. Chang, H.H. Wang, S.Y. Chen, C.A. Lin, S.A. Chen, Y.L. Chueh, J.H. He, ACS Nano 5 (2011) 9501–9510.
[30] S.-F. Leung, L. Gu, Q. Zhang, K.-H. Tsui, J.-M. Shieh, C.-H. Shen, T.-H. Hsiao, C.-H. Hsu, L. Lu, D. Li, Sci. Rep. 4 (2014) 4243.
[31] S.-F. Leung, K.-H. Tsui, Q. Lin, H. Huang, L. Lu, J.-M. Shieh, C.-H. Shen, C.-H. Hsu, Q. Zhang, D. Li, Energy Environ. Sci. 7 (2014) 3611–3616.
[32] J.H. Ahn, H.S. Kim, K.J. Lee, S. Jeon, S.J. Kang, Y.G. Sun, R.G. Nuzzo, J.A. Rogers, J. A. Science 314 (2006) 1754–1757.
[33] F.-R. Fan, Z.-Q. Tian, Z.L. Wang, Nano Energy 1 (2012) 328–334.
[34] C. Zhang, Z.L. Wang, Nano Today 11 (2016) 521–536.
[35] X. Pu, M.M. Liu, X.Y. Chen, J.M. Sun, C.H. Du, Y. Zhang, J.Y. Zhai, W.G. Hu, Z.L. Wang, Sci Adv 3 (2017) 1700015.
[36] S.F. Leung, K.T. Ho, P.K. Kung, V.K.S. Hsiao, H.N. Alshareef, Z.L. Wang, J.H. He, Adv. Mater. 30 (2018) 1704611.
[37] Z.H. Lin, G. Cheng, Y. Yang, Y.S. Zhou, S. Lee, Z.L. Wang, Adv. Funct. Mater. 24 (2014) 2810–2816.
[38] L.T. Dou, A.B. Wong, Y. Yu, M.L. Lai, N. Kornienko, S.W. Eaton, A. Fu, C.G. Bischak, J. Ma, T.N. Ding, N.S. Ginsberg, L.W. Wang, A.P. Alivisatos, P.D. Yang, Science 349 (2015) 1518–1521.
[39] M.I. Saidaminov, O.F. Mohammed, O.M. Bakr, Acs Energy Lett 2 (2017) 889–896.
[40] S.M. Niu, S.H. Wang, L. Lin, Y. Liu, Y.S. Zhou, Y.F. Hu, Z.L. Wang, Energy Environ. Sci. 6 (2013) 3576–3583.
[41] F.R. Fan, J.J. Luo, W. Tang, C.Y. Li, C.P. Zhang, Z.Q. Tian, Z.L. Wang, J. Mater. Chem. 2 (2014) 13219–13225.
[42] S.H. Wang, L. Lin, Z.L. Wang, Nano Lett. 12 (2012) 6339–6346.
[43] L. Su, Z.X. Zhao, H.Y. Li, J. Yuan, Z.L. Wang, G.Z. Cao, G. Zhu, ACS Nano 9 (2015) 11310–11316.
[44] P.A. Shaikh, D. Shi, J.R.D. Retamal, A.D. Sheikh, M.A. Haque, C.F. Kang, J.-H. He, O.M. Bakr, T. Wu, J. Mater. Chem. C 4 (2016) 8304–8312.
[45] S. Silver, J. Yin, H. Li, J.L. Bredas, A. Kahn, Adv. Energy Mater. 8 (2018) 1703468.
[46] D.L. Shao, M.P. Yu, H.T. Sun, T. Hu, J. Lian, S. Sawyer, Nanoscale 5 (2013) 3664–3667.
[47] Z.L. Wang, J. Chen, L. Lin, Energy Environ. Sci. 8 (2015) 2250–2282.

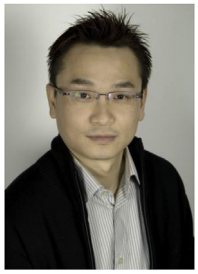

Dr. Vincent K. S. Hsiao received Ph. D. from the Department of Electronic Engineering, University at Buffalo. He served as Assistant Professor in the year of 2007 from the Department of Applied Materials and Optoelectronic Engineering, National Chi Nan University, Taiwan, and was promoted as Professor in the year of 2013. His current researches are mainly focusing on Photonics, Photothermoelectronics, Laser-assisted fabrication of nanomaterials, and Laser spectroscopy.

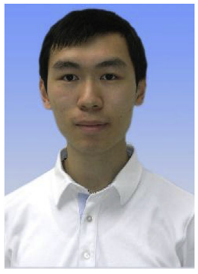

Dr. Siu-Fung Leung received his PhD degree in Nano Science and Technology at Hong Kong University of Science and Technology and currently is a Research Fellow at Australian National University. His research interest is on functional nanomaterials and their applications in renewable energy and functional coating.

Yung-Chi Hsiao was a graduate student in Materials Science and Engineering Department at National Chung Hsing University, Taiwan. His advisor for master thesis was Prof Ying-Chih Lai. He received his master degree in the year of 2018. His former research is triboelectric nanogenerator (TENG) related flexible/stretchable/wearable electronics.

Po-Kai Kung is a PhD student supervised by Prof. Peter Chen in National Cheng Kung University (NCKU). He received his BS (2014) and MS (2017) degree in Material Science Engineering from NCKU. Before joining Prof. Chen's team, he was also a visiting scholar supervised by Prof. Jr-Hau He in King Abdullah University of Science and Technology (KAUST). During his time as a master student, he has carried out studies of 2D material synthesis and related photovoltaic application. His current research interest is lead free perovskite solar cell.

Dr. Ying-Chih Lai currently is an Associate Professor of Materials Science and Engineering Department at National Chung Hsing University in Taiwan. He received his B.S. in Materials Science and Engineering (minor in electrophysics) from National Chiao Tung University and his M.S. and Ph.D. in Electronic Engineering from National Taiwan University. His research interests include self-powered sensors, nanogenerators, electronic skins, soft robotics, and flexible/stretchable/wearable electronics.

Dr. Zong-Hong Lin is currently an Associate Professor in Institute of Biomedical Engineering and Department of Power Mechanical Engineering, National Tsing Hua University. His research interests include the development of high-output nanogenerators with smart designs, self-powered systems as biomedical and environmental sensors, highly efficient and stable catalysts for electrochemical applications, and functional nanomaterials for controlled antibacterial activity.

Dr. Jr-Hau He is an Associate Professor of Electrical Engineering program at King Abdullah University of Science & Technology (KAUST). He has been a pioneer in optoelectronics, which reflects on his achievement of photon management on the light harvesting devices. He has conducted highly interdisciplinary researches to bridge those gaps between various research fields and between academia and industry. He is a Fellow of OSA, RSC and SPIE, and a senior member of IEEE. Visit his web for more information (nanoenergy.kaust.edu.sa).

Dr. Husam N. Alshareef is a Professor of Materials Science & Engineering at KAUST. After nearly ten years in the semiconductor industry, he joined KAUST in 2009 where he initiated an active research group working on inorganic nanomaterial development for energy storage and emerging electronics. Prof. Alshareef is a Fellow of the Royal Society of Chemistry, IEEE Distinguished Speaker in Nanotechnology, and Senior Member of IEEE.

Dr. Khaled N. Salama received his masters and doctorate degrees from the Electrical Engineering Department at Stanford University. His work on CMOS sensors for molecular detection was awarded the Stanford-Berkeley Innovators Challenge Award in biological sciences and was acquired by Lumina Inc in 2008. He was an assistant professor at RPI between 2005 and 2008. He is a Professor and founding chair member in the Electrical engineering department at King Abduallah University of Science and Technology. He is currently the director of the sensor initiative at KAUST. He is the co-author of 200 papers and 14 patents on sensors.

Prof. Zhong Lin Wang received his Ph.D. from Arizona State University in physics. He now is the Hightower Chair in Materials Science and Engineering, Regents' Professor, Engineering Distinguished Professor and Director, Center for Nanostructure Characterization, at Georgia Tech. Dr. Wang has made original and innovative contributions to the synthesis, discovery, characterization and understanding of fundamental physical properties of oxide nanobelts and nanowires, as well as applications of nanowires in energy sciences, electronics, optoelectronics and biological science. His discovery and breakthroughs in developing nanogenerators established the principle and technological road map for harvesting mechanical energy from environment and biological systems for powering personal electronics. His research on self-powered nanosystems has inspired the worldwide effort in academia and industry for studying energy for micro-nano-systems, which is now a distinct disciplinary in energy research and future sensor networks. He coined and pioneered the field of piezotronics and piezophototronics by introducing piezoelectric potential gated charge transport process in fabricating new electronic and optoelectronic devices. Details can be found at: http://www.nanoscience.gatech.edu.